April 2011

The Correlation of Mass-Burning Rate of Condensed Fuels to Temperature Gradient at the Fuel Surface

Eric Michael Camiel
Worcester Polytechnic Institute

The Correlation of Mass-Burning Rate of Condensed Fuels to Temperature Gradient at the Fuel Surface

A Major Qualifying Project
Submitted to the faculty of Worcester Polytechnic Institute in partial fulfillment of the requirements for the Degree of Bachelor of Science in Mechanical Engineering

Submitted by:
Eric Camiel

April 28th 2010

Report submitted to:

Professor Ali Rangwala
Fire Protection Engineering
Worcester Polytechnic Institute

Abstract:

Currently, there are many unknowns regarding fire and its behavior. Fire is constantly being investigated to better understand its fundamentals both in large and small scale research. This project explores the relationship that exists between the mass-burning rate of condensed fuels and the gas-phase temperature gradient in the space between a burning surface and the flame front. A thermocouple probe was specially designed to collect temperature data and consisted of a 0.0762mm diameter unsheathed fine gage thermocouple that is supported and protected by ceramic insulating tubing. A noncombustible porous brick was used such that combustion of a liquid fuel was supported on one brick face as it diffused through the porous material. The liquid fuel was supplied at a constant and controlled rate to ensure a steady mass-loss rate. To measure the temperature gradient in the laminar boundary layer of the combustion film along the entire height of the fuel brick, the thermocouple probe was moved in both the vertical and horizontal directions by increments of 0.1mm to 10mm. Currently, this correlation is supported with numerical models validated by applicable, but inexplicit experimental data. The experiments in this project were specifically designed to explicitly support the correlation of gas-phase temperature gradient in the space between a burning surface and the flame front along the entire height of a vertical burning surface.

Acknowledgements:

I would like to thank the following individuals who dedicated their time and effort to aid in my research and completion of my Major Qualifying Project at Worcester Polytechnic Institute.

Ali Rangwala
Professor
Fire Protection Engineering
Worcester Polytechnic Institute

Scott Rockwell
PHD Student
Fire Protection Engineering
Worcester Polytechnic Institute

Table of Contents

Table of Figures

Table of Equations

1. Introduction:

Fire protection engineering is a relatively young area of study compared to other engineering sciences. There is still much to be discovered and understood about fire and its fundamentals. Because of this, research is continuously being done to better understand fire and its behavior. This research includes both large and small-scale studies. Current building and fire codes rely on the research that has already been completed in order to make scientific recommendations for protecting people, property and structures from fire. Because fire research is ongoing, the codes and standards are constantly changing. This fundamental research is vital to the development of fire protection as a science and to the overall safety of society. The current study explores the correlation of two fundamental properties of fire and can be classified under the small-scale research realm. These fundamental properties are the mass-burning rate of a fuel and the temperature gradient at the fuel surface of a burning fuel.

2. Background:

The mass-burning rate of any fuel is an important fundamental characteristic to know when studying fire dynamics. From it, heat release rates and flame-spread properties can be calculated and used in many fire-engineering applications. These properties are vital in the understanding of fire behavior and in the classification fire hazards. Fire protection codes and standards such as NFPA 13-*Standard for the installation of sprinkler Systems* rely on these properties (1). Specifically, the heat release rates of fuels are used to determine the level of hazard being protected (1). However, it is not always easy or feasible to accurately measure the mass-burning rates of fuels.

A paper titled "*Estimation of Laminar Mass Burning Rate of a Condensed Fuel using Temperature Field*" proposes that the local mass-burning rate per unit area along a fuel surface can be correlated to the temperature gradient taken at the fuel surface (2). Although this paper utilizes numerical models in order to support the relationship, these numerical models have been validated by applicable but inexplicit experimental data (2). Additionally, the paper supports this correlation for a variety of fuel surface orientation angles. However, for the purposes of this study, only the vertical or 90° orientation will be considered.

This study attempts to experimentally validate the correlation of the mass-burning rate of a condensed liquid fuel to the temperature gradient at the surface of the burning fuel. The mass-burning rate can be defined as the rate of which mass is lost due to the combustion of the fuel. Additionally, the temperature gradient at the fuel surface can be defined as the rate of change of the temperature from the fuel surface toward the flame. This temperature gradient exists in the gas-phase zone of a diffusion flame as shown in Figure 1: Gas-Phase Temperature Gradient

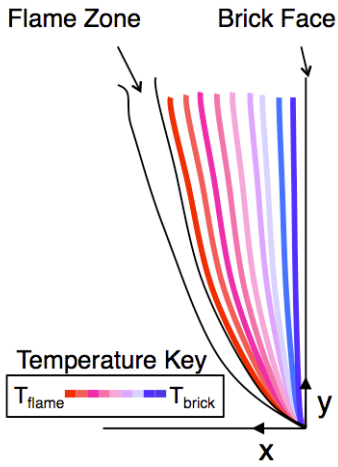

Figure 1: Gas-Phase Temperature Gradient

The correlation proposed in the paper is shown below in Equation 1: Correlating Equation (2).

$$\dot{m}''_f = \frac{c}{L}\left(\frac{\partial T^*}{\partial x^*}\right)_{x^*=0}\left(\frac{kg}{m.s}\right)$$

Equation 1: Correlating Equation

This equation includes a constant c that is defied by Equation 2 below where B is the mass-transfer number, k is the thermal conductivity of the fuel in its gaseous phase and C_p is the specific heat of the fuel in its gaseous phase. L is defined as the length of the burning fuel surface and $\frac{dT^*}{dx^*}$ is the nondimensional temperature gradient. The nondimensional temperature and nondimensional x values are defined by Equation 3 where T is the actual temperature, T_∞ is the ambient temperature, x is the position along the x axis within the gas-phase zone and L is the overall length of the burning surface (2).

$$c = \left(\frac{B \times k}{C_p}\right)\left(\frac{kg}{m.s}\right)$$

Equation 2: Constant C Equation

$$T^* = \frac{T - T_\infty}{T_\infty} \quad x^* = \frac{x}{L}$$

Equation 3: Nondimensional Values

Since the mass-burning rate varies along the length of a burning surface, this correlation will yield the surface mass-burning rate at a specific location along the length of the fuel. If this value is known for multiple points along the fuel length, these local mass-burning rate values may be integrated over the fuel length to yield a mass-burning rate per unit length. Furthermore, this mass-burning rate per unit length may be multiplied by the width of the fuel surface to yield a total mass-burning rate over the entire fuel surface.

3. Experimental Setup

In order to use this correlation, knowledge of the temperature profile in the fuel diffusion zone is necessary. This section will explain the design and setup of the instrumentation as well as the process of data collection for the experiments. The following sections are as follows:

0 – Fuel Burning Apparatus

0 – Temperature Probe

3.3 – Fuel Feeding Mechanism

3.4 – Data Acquisition

3.1 Fuel Burning Apparatus

As stated before, the vertical fuel orientation was the focus of this study. The first challenge of designing the liquid fuel burning apparatus was developing a means to burn liquid fuel along a vertical surface. To accomplish this, a porous noncombustible material was selected such that it would allow the fuel to freely diffuse through it while being able to withstand the high temperatures of an open flame. Since the experiment relied on the accurate measurement of the mass-loss of the liquid fuel, it was important that the porous material would not decompose or lose mass when exposed to the high temperature conditions during the combustion of the fuel. Also, part of the material selection criteria included the structural integrity at high temperatures. It was vital that the material provided a constant surface area for the fuel to diffuse through.

A material that consisted of 90% air and 10% silica fibers was selected. This technology was developed by NASA and was used on the exterior of space shuttles for its ability to withstand temperatures of up to 2,300°F (3). A brick of this material was partially enclosed by 20-gage steel such that it was supported in a vertical position. A surface measuring 65mm in height and 55mm in width was left unenclosed to serve as the area for combustion of the liquid fuel. Copper tubing was fed through the top of the sheet metal enclosure and inserted into the top

of the brick. This supply tubing injected the liquid fuel into the brick. From there it was allowed to freely soak into the porous material creating a vertical liquid fuel surface.

Once the copper fuel supply tubing was in place, the back of the brick was sealed to the sheet metal with high temperature ceramic cement. The top of the brick was also sealed around the copper supply tubing with high temperature cement. Additionally, the open back of the sheet metal enclosure was sealed using aluminum tape. The brick was sealed so that fuel vapor would not escape preventing combustion in areas other than the open brick face. A labeled picture of the fuel burning apparatus can be seen in Figure 2: Fuel Burning Apparatusbelow.

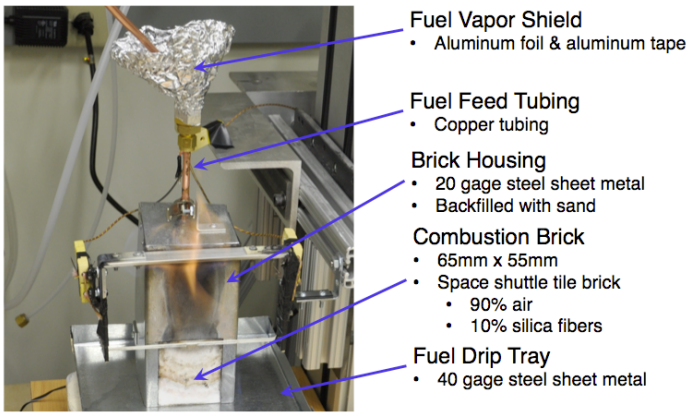

Figure 2: Fuel Burning Apparatus

The funnel–like aluminum foil seen in Figure 2: Fuel Burning Apparatus serves as a shield for the vapors that may escape when the fuel is fed into the burning apparatus. It should be noted that the copper supply tubing running into the aluminum foil vapor shield does not make contact with the fuel burning apparatus. This externally supported tubing is fed to the funnel where the fuel drips into the supply piping of the burning apparatus. It was necessary for the fuel burning apparatus to be freestanding because the load cell precisely measured the mass-burning rate of the entire apparatus. External contact of any kind would have voided the mass-loss data. Also seen in Figure 2: Fuel Burning Apparatus, the burning apparatus is sitting on a metal drip tray. This drip tray collected any excess fuel in the case that the brick was oversaturated.

3.2 Temperature Probe

Once the fuel burning apparatus was designed and constructed, a means to measure temperature at precise locations along the brick was developed. For this, a temperature probe was designed. This temperature probe needed to be able to accurately measure temperature in the fuel diffusion zone of the flame. Additionally, in order to collect the necessary data, the probe needed to have the freedom to move along both the x and y axis of the brick. Additionally, it was necessary that it was able to withstand the high temperatures that exist near the burning fuel.

Type K thermocouples were chosen to record the temperature data. Since the temperature measurements had to be extremely accurate, fine gage thermocouples were chosen, as their pinpoint accuracy is much greater than other types of thermocouples. Thermocouples of diameters varying from 0.0127mm to 0.0762 mm were experimented with. The thinner diameter thermocouples proved to be a significant challenge to work with due to their miniscule size. Additionally, the 0.0127mm thermocouples could not be exposed to an open flame. It was observed that they would break when directly exposed to a flame for more than a few seconds. From these trials, it was decided that the larger diameter thermocouples within the selected range would work best as they were more robust and resistant to flames while still providing extremely accurate temperature data.

Once the type and size of the thermocouple were chosen, a mechanism was designed to support the thin thermocouple wire. Ceramic insulating tubing was chosen to provide structural support to and heat resistance around the thermocouple wire. Figure 3: Temperature Probeshows the constructed thermocouple probe.

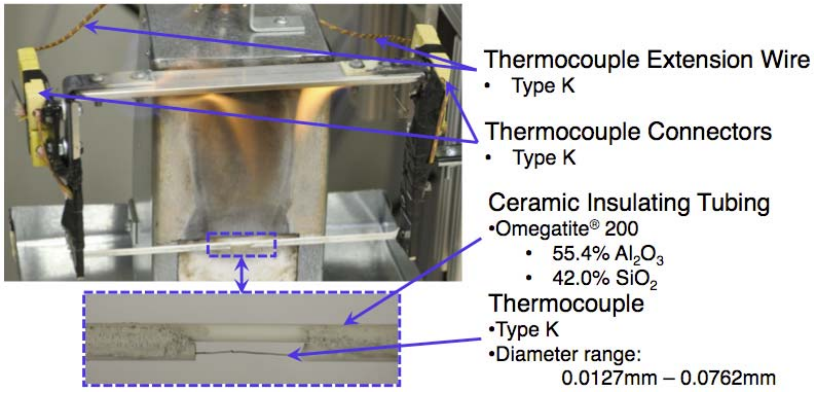

Figure 3: Temperature Probe

The ceramic tubing was rated to withstand temperatures of up to 3000°F. It was constructed of a material called Omegatite® 200 and was comprised of mostly Al_2O_3 and SiO_2 in the respective concentrations of 55.4% and 42.0% (4).As seen in Figure 3: Temperature Probe, two shorter tubes were cemented to one longer tube leaving a space for the thermocouple bead in the center of this opening. The space allowed the thermocouple bead to be exposed to the surrounding environment and accurately record the temperature. The ceramic tubing was fixtured to metal framing that served as the connection to the axis control system. The cement used to adhere the ceramic tubing together and to the metal support frame was of the high temperature rating. This CC series thermocouple cement was rated for a maximum service temperature of 1550°C (5).

The temperature probe framing also housed the thermocouple connectors for the extension wires to the data acquisition device. These connectors allowed the probe to be easily detached for repair and maintenance.

3.3 Fuel Feeding Mechanism

For the mass-burning rate to be accurately measured, it was necessary that the fuel supply rate be held constant. Because the mass-burning rate is a constant value, it could easily be calculated from the load cell data. By taking the measured mass-loss rate of the load cell and

adding the constant supply rate, the total mass-burning rate was arrived at. **Error! Reference source not found.** shows the mass balance for the system. When the fuel is burning, $\frac{dm}{dt}$ is negative since the system is losing mass. The mass-loss rate $\frac{dm}{dt}$, was observed to be constant at -0.0529g/s. This rate is negative because the mass-burning rate was larger than the fuel supply rate. The fuel supply rate, $\dot{m}_{in}$, was set at 0.0251g/s (estimated from the load cell data with no burning). This rate is positive since it is the fuel supply rate into the brick. The total mass-burning rate $\dot{m}_{out}$, can be calculated per Equation 4 as -0.078g/s. This rate is also negative since it is the rate at which the fuel is burning.

$$\frac{dm}{dt} = \dot{m}_{in} - \dot{m}_{out} \quad \xrightarrow{yields} \quad \dot{m}_{out} = \left|\frac{dm}{dt}\right| + \dot{m}_{in}$$

Equation 4: System Mass Balance

In order to keep the fuel supply rate constant, an "IV" style system was constructed. It consisted of a 1-liter dry bag with plastic tubing leading into a 25mL burette. A control valve was installed on the supply tubing such that the fuel supply could easily be terminated at any point during the experiment. Every component of this fuel supply system was interconnected in an airtight fashion. The bottom opening of the burette was the only opening to the atmosphere. This airtight configuration ensured that as fuel flowed out of the burette, fuel was also supplied into the burette at the same rate. Because of this, the level of fuel in the burette was kept constant. This constant pressure head in the burette ensured that the fuel supply remained constant. Figure 4 shows the setup of the fuel feeding mechanism.

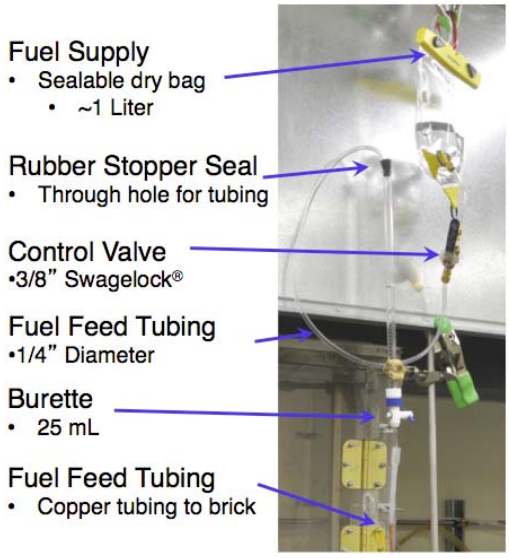

Figure 4: Fuel Feeding Mechanism

As seen in Figure 4, copper tubing transported the fuel to the brick supply tubing as it flowed out of the bottom of the burette. As stated before, this transport tubing was installed such that it did not make contact with the fuel burning apparatus.

3.4 Data Acquisition

Both mass-loss data and temperature data were collected during the experiment. The load cell was connected to a computer that continuously measured the mass-loss data over the entire duration of the experiment. The thermocouple probe was also connected to a data acquisition program on the computer and recorded temperature data for 20 seconds at each measurement point. Temperature data was taken at 2 measurements per second and a total of 40 temperature values were collected at each measurement point. The average value of these 40 measurements for each point along the brick was used in the data analysis. Figure 5 shows where the temperature measurement points were along the brick face.

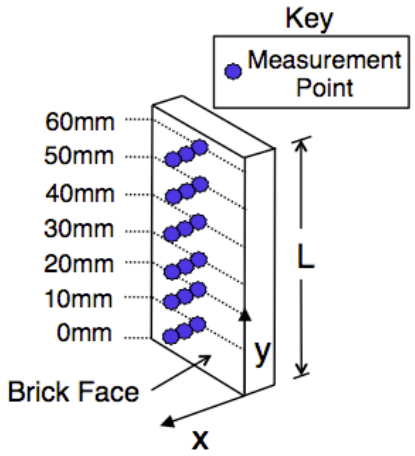

Figure 5: Temperature Measurement Points

3.4.1 Experimental Procedure

Experiments were run using ethanol as fuel. Shown below is the experimental procedure that was followed in each experiment.

1. 1-liter dry bag of was filled with ethanol and sealed
2. Load cell data acquisition was initiated
3. Control valve was opened to initiate fuel supply to brick
4. Brick face was ignited after brick was saturated
5. Temperature probe was moved to measurement point
6. Temperature data was collected
7. 5 and 6 were repeated until all temperature data was collected
8. Fuel supply was terminated
9. Load cell data acquisition was terminated
10. Remaining fuel was allowed to burn off

It should be noted that the experiments were carried out underneath a fume hood that collected the combustion byproducts. Additionally, a nitrogen gas hose line was kept charged in the case of emergency extinguishment. A CO_2 fire extinguisher was also kept on hand as a last resort if the nitrogen gas could not extinguish the fire.

4. Results

Figure 6 shows the temperature curves at each measurement height of the brick. It should be noted that the brick temperature was assumed to be constant at 74°C. This temperature is just below the boiling point of ethanol. The assumed temperature of 74°C is assuming that there is a thin ethanol film on the brick face. This film is close to the boiling point of the fuel however, because it is liquid, the temperature just below the actual boiling point. Another observation from Figure 6 is that the temperature measurements begin at a distance of 2.54mm. This minimum distance is due to limits in the construction of the instrumentation. Assuming the thermocouple probe is in the center of the ceramic tubing, the minimum distance away from any surface that the probe can be is equal to the radius of the tubing. Additionally, since the brick was partially enclosed by 20-gage sheet metal, the thickness of the sheet metal also restricts the probe movement in the x direction. The thickness of the sheet metal is 0.9525mm and the radius of the tubing is 1.5875mm resulting in a minimum measurement distance in the X direction of 2.54mm away from the brick face.

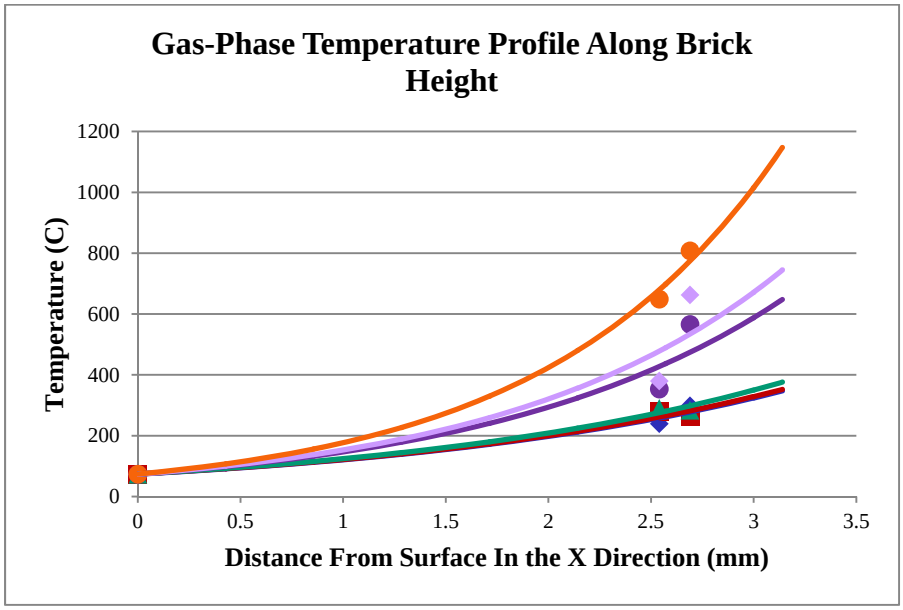

Figure 6: Gas-Phase Temperature Curves

It can be seen from Figure 6 that as the probe moved away from the fuel surface, the temperature exponentially increased. This was because as the distance from the fuel surface increases, the temperature of the gas-phase zone also increases as it approaches the flame temperature. Figure 1 further clarifies this temperature profile that exists in the gas-phase zone of a diffusion flame. Furthermore, it can be seen that as the probe moved closer to the base of the brick, the temperature increased more quickly along the X-axis. This is because there is less of a flame standoff distance from the brick at this lower height. The temperature of the gas-phase zone approaches the flame temperature over a shorter distance than at the higher measurement points on the brick face. Figure 7 shows this flame standoff distance along the brick face.

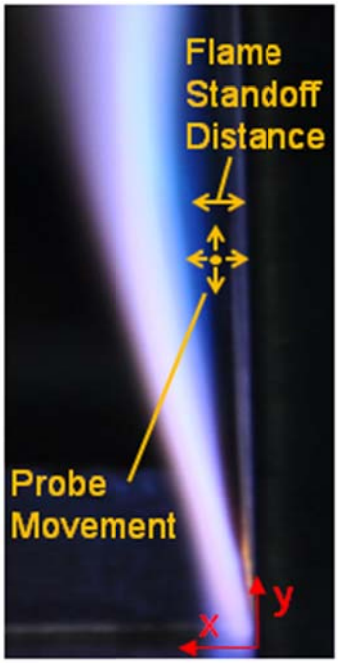

Figure 7: Flame Standoff Distance and Probe Movement Directions

The next step in the data analysis was to determine the corresponding temperature gradient curve from the temperature profile curves in Figure 6. This was done by differentiating the exponential temperature trend lines at the fuel surface or X = 0. The resulting temperature

gradient curve is shown in Figure 8: Fuel Surface Temperature Gradient Along Brick Height where T is in Kelvin.

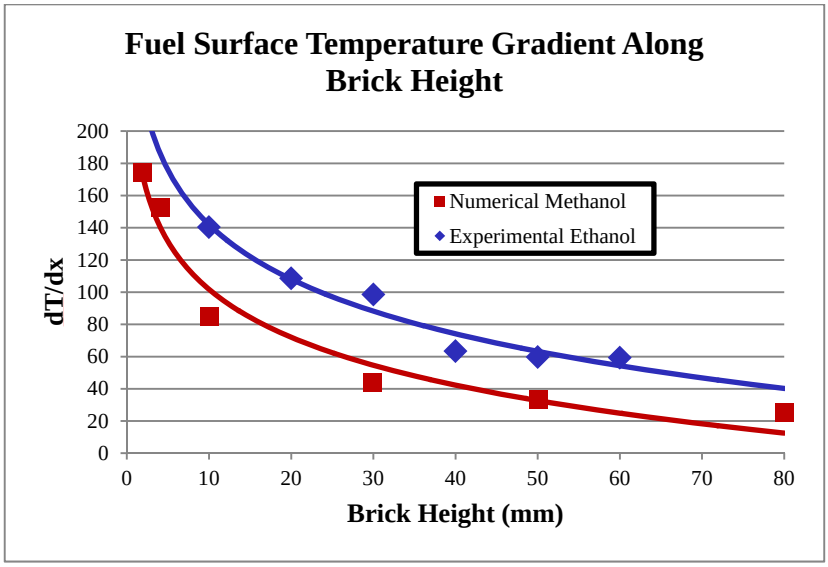

Figure 8: Fuel Surface Temperature Gradient Along Brick Height

Since the original paper used methanol as a fuel, the temperature gradient curves of both the numerical methanol data and the current experimental data for ethanol can be compared (2). As seen in Figure 8, the temperature gradient curves for both the numerical methanol and experimental ethanol data follow the same trend. Since the correlation equation (Equation 1) is a constant multiple of the nondimensional temperature gradient, this agreement in trend gave promise to the accuracy of the correlating equation.

Once the temperature gradient curves were derived, they had to be converted into the nondimensional form. As was stated in the background section, the nondimensional quantities were substituted as per Equation 3. Once this nondimensional temperature gradient curve was determined, it could then be used in the correlating equation to calculate the corresponding local mass-burning rate per unit area curve. However, the correlating equation also relied on the calculation of the constant *c* as previously defined by Equation 2.

The mass transfer number (*B*) was calculated as 4.1, the thermal conductivity of the gas-phase zone was taken as 0.61W/m-K and the specific heat of the gas phase zone was taken as 1450 J/Kg-K (6) (2). These values were determined using the scheme explained in an article entitled "*A new property evaluation scheme for mass transfer analysis in fire problems*" (7). The specific heat value was taken as the specific heat of standard air at the adiabatic flame temperature of ethanol. Similarly, the thermal conductivity of the gas-phase zone was taken as the thermal conductivity of standard air at a temperature T_{avg} which is represented by Equation 5 (7). From these values, the constant *c* was calculated as 0.1725g/m-s.

$$T_{avg} = \frac{T_\infty - T_f}{3}$$

Equation 5: Average Temperature for Calculating k

Multiplying the nondimensional temperature gradient curve by the constant *c/L* per Equation 2 where L = 0.065mm, yields a local mass-burning rate per unit area curve along the length of the brick. This local-mass burning rate curve is shown below in Figure 9**.**

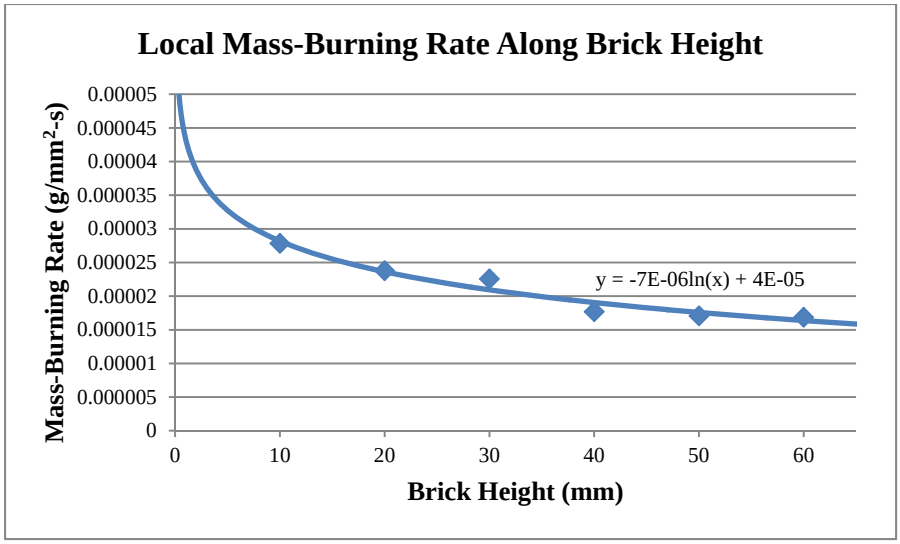

Figure 9: Local Mass-Burning Rate Along Brick Height

In order to obtain a total mass-burning rate, this local mass-burning rate curve must first be integrated over the height of the brick. Doing so yields a mass-burning rate per unit width of

the fuel surface. Multiplying this mass-burning rate per unit width value by the width of the brick of 55mm yields a total mass-burning rate in g/s. This total mass-burning rate value was calculated at 0.0635 g/s. See appendix B for the specific calculations.

5. Discussion

The calculated mass-burning rate of 0.0635g/s is compared to the actual mass-burning rate determined from the load cell data per Equation 4. This total mass-burning rate was 0.078g/s. The difference of the calculated value and the measured value is 0.0145g/s which translates to a difference of 18.6%. There are many factors that could have affected the experiment and caused this difference in the measured and calculated values. However, due to the difficulty in taking precise temperature measurements, the difference of 18.6% is acceptable.

One factor that may have contributed to this discrepancy is the escape of fuel vapors from the fuel burning apparatus. During the experiments, fuel vapor was observed exiting the fuel burning apparatus near the top and bottom of the enclosure. This vapor was ignited by the open flame on the brick face and contributed to the overall mass-loss rate. Since the temperature measurements were taken at specific points along the brick face and this additional vapor combustion occurred in areas other than the brick face, the corresponding mass-loss from the vapor combustion was not accounted for in the temperature measurements. Since the entire burning apparatus sat on the load cell, the mass-loss data incorporated this burning vapor. This certainly contributed to a higher measured mass-loss value compared to the calculated value.

Another factor that may have contributed to this difference is the fact that conduction and radiation losses from the thermocouple wire were assumed to be negligible. However, if these losses were significant, the measured temperatures would be significantly lower than the actual

temperatures in the gas-phase zone. If these temperatures were higher, the slope of the exponential trend lines in Figure 6 would increase. This would contribute to a larger temperature gradient value. Since the correlation equation directly relates the temperature gradient to the mass-burning rate, if the temperature gradient values are increased, the mass-burning rate values would also increase.

Additionally, the assumption that the brick surface remained a constant temperature at a value just below the boiling point of ethanol may be invalid. If this temperature is different than the assumed value, the temperatures curves in Figure 6 will be different. This would also lead to different values of the fuel surface temperature gradient thus further resulting in differences of the corresponding mass-burning rate.

6. Conclusion

Overall, since the correlating equation relates the temperature gradient to the mass-burning rate of various condensed fuels, the experimental results of this study for ethanol can be compared to the numerical model results for methanol included in the original paper (2). From Figure 8 it can be seen that the temperature gradient curves of both studies agree in terms of their overall trend line shape. Due to this agreement and since the correlation has been supported for methanol by applicable data, it can be concluded that the correlating equation is applicable in predicting the local mass-burning rates of an ethanol fuel surface.

Furthermore, the accuracy of the correlating equation can be supported by the fact that the measured and calculated values of this study were within 20%. Considering the margin for error in the measurements and the assumptions that were made, this 18.6% difference is acceptable. It can be concluded that the correlation equation of the mass-burning rate of a condensed fuel to the temperature gradient at the fuel surface is supported by both the inexplicit numerical data for methanol and the explicit experimental data for ethanol in this study. Thus, this correlation should hold true for other condensed liquid fuels.

Works Cited

1. Lake, James D. *NFPA 13 Standard for the Installation of Sprinkler Systems.* Quincy : NFPA, 2010.

2. *Estimation of Laminar Mass Burning Rate of a Condensed Fuel using Temperature Field.* Ali, Seik Mansoor, Raghavan, Vasudevan and Rangwala, Ali S.

3. NASA. NSTS 1988 News Reference Manual. *Space Shuttle Orbiter Systems.* [Online] 1988. [Cited: April 22, 2011.] http://science.ksc.nasa.gov/shuttle/technology/sts-newsref/sts_sys.html.

4. Omega Engineering. Ceramic Thermocouple Insulators. [Online] [Cited: April 23, 2011.] http://www.omega.com/pptst/ORX_INSULATORS.html.

5. Omega Engineering. OMEGABOND High Temperature Chemical Set Cements. [Online] [Cited: April 27, 2011.] http://www.omega.com/Temperature/pdf/OB_BOND_CHEM_SET.pdf.

6. Engineering Toolbox. The Engineering Toolbox. *Dry Air Properties.* [Online] [Cited: April 25, 2011.] http://www.engineeringtoolbox.com/dry-air-properties-d_973.html.

7. *A new property evaluation scheme for mass transfer analysis in fire problems.* Rangwala, Ali S., Raghavan, Vasudevan, Sipe, Joel E., Okano,Terumi. Fire Safety Journal 44, pp. 652-658.

Appendix A: Project Poster

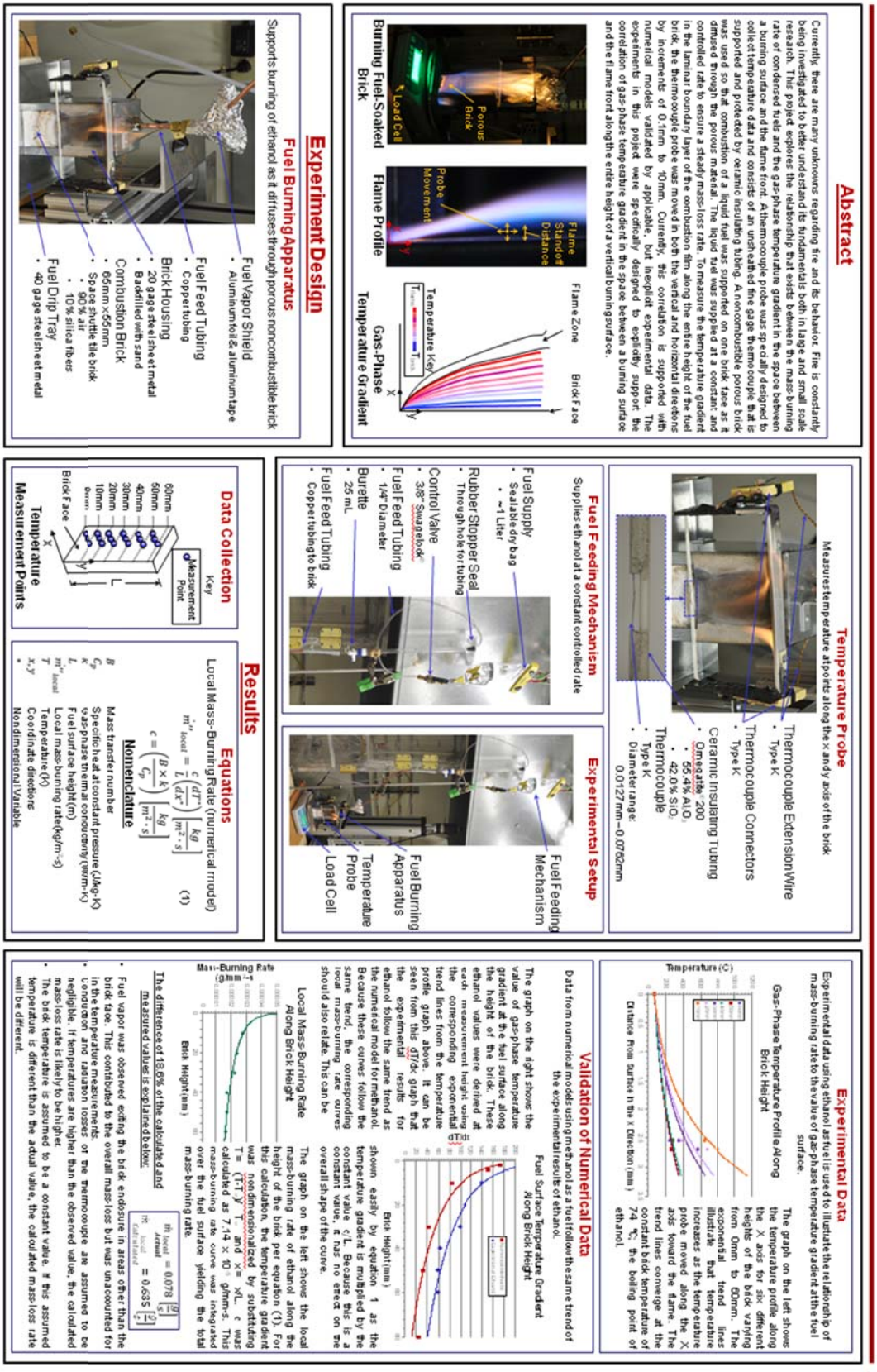

Appendix B: Mass-Burning Rate Calculations

c = 0.1725g/m-s = .0001725g/mm-s

L = 65mm

$\frac{c}{L}$ = 2.654 x 10^{-6} g/mm^2-s

$\frac{dT^*}{dx^*} \times \frac{c}{L}$ = Local mass burning rate per area curve from Figure 9

The logarithmic trend line of this curve is: y = -7 x 10^{-6} ln(x) + 4 x 10^{-5}

Integrating over the brick height (L):

$$\int_{0mm}^{65mm} (-7 \text{ x } 10 - 6 \ln(\text{x}) + 4 \text{ x } 10 - 5) \, \text{dx} = 1.155 \times 10^{-3} \left[\frac{g}{mm - s}\right]$$

*Mathcad was used to evaluate the above integral

Multiplying by the brick width of 55mm:

$$1.155 \times 10^{-3} \times 55mm = 0.0635 \left[\frac{g}{s}\right]$$

0.0635 g/s is the total calculated mass-burning rate.